Low-energy electron scattering by H_2O, H_2S, H_2Se, and H_2Te

Márcio T. do N. Varella
Instituto de Física Gleb Wataghin, Universidade Estadual de Campinas (UNICAMP), 13083-970 Campinas, São Paulo, Brazil

Márcio H. F. Bettega
Departamento de Física, Universidade Federal do Paraná (UFPR), Caixa Postal 19081, 81531-990 Curitiba, Paraná, Brazil

Marco A. P. Lima and Luiz G. Ferreira
Instituto de Física Gleb Wataghin, Universidade Estadual de Campinas (UNICAMP), 13083-970 Campinas, São Paulo, Brazil

(Received 19 August 1998; accepted 15 July 1999)

We report elastic differential, integral, and momentum transfer cross-sections for H_2X molecules (X: O, S, Se, and Te) obtained at the static exchange level of approximation. The energy range considered was from 2 up to 30 eV for H_2O and from 5 up to 30 eV for the other molecules. Our calculations were performed with the Schwinger multichannel method with pseudopotentials [M. H. F. Bettega, L. G. Ferreira, and M. A. P. Lima, Phys. Rev. A **47**, 1111 (1993)], combined with a Born closure procedure in order to account for the long-range potential due to the permanent dipole moment of the targets. Our calculated cross-sections for H_2O and H_2S are in good agreement with other theoretical results. Agreement with available experimental data is also encouraging. It was found that molecular size plays a crucial role in the scattering process. The influence of heavy and H atoms in the collisions is also discussed. For the integral cross-sections of the heavier molecules we also investigated incident energies below 5 eV, looking for possible shape resonances. Through the symmetry decomposition of the integral cross-sections and the eigenphase sum analysis, we found shape resonances for H_2S, H_2Se, and H_2Te at the B_2 symmetry. For H_2Te, we have also found a shape resonance at the A_2 symmetry. For all molecules a very broad structure was found at the A_1 symmetry. This is the first work to report such resonances for H_2Se and H_2Te. © *1999 American Institute of Physics.* [S0021-9606(99)01438-5]

I. INTRODUCTION

The excitation of molecular targets by low-energy electrons is an important energy-loss mechanism in molecular gases, playing a relevant role in determining the electron-velocity distribution in a gaseous discharge, in electron drift experiments, and in the ionosphere of Earth and other planets.[1] One may also find technological processes, such as the description of cold plasma,[2] in which e^--molecule collisions are of interest. It follows that the knowledge of elastic and inelastic cross-sections for a wide range of molecular systems is a very important subject.

In the past few years, the Schwinger multichannel method with pseudopotentials (SMCPP)[3] has been applied to calculate elastic[4,5] and rotationally inelastic[6–8] cross-sections for electron scattering by molecules of arbitrary geometry. The SMCPP is an entirely *ab initio* method and uses only square-integrable functions (Cartesian Gaussian functions) to represent the scattering eigenfunctions. When the molecular targets have many electrons, however, *ab initio* calculations quickly run into computational limitations, due to the need for very large basis sets. The use of norm-conserving pseudopotentials (PP), however, considerably reduces the computational effort. In the SMCPP approach, only the valence electrons are described in a usual many-body framework (Hatree–Fock approximation in our case), the core electrons being replaced by the PP. Since we use the norm-conserving PP of Bachelet, Haman, and Schlüter (BHS),[9] our pseudowave-functions are nodeless and smooth. Reduced basis sets result because of the following basic reasons: (i) there is no need to take core electrons into account, and (ii) there are no nodes in the pseudowavefunctions to be described. The use of BHS pseudopotentials also brings the advantage of incorporating relativistic corrections, which are important for heavier atoms.

The SMCPP procedure has allowed calculations of elastic and rotationally inelastic cross-sections for heavier targets, such as XH_4 (X: C, Si, Ge, Sn, and Pb),[6,10] XH_3 (X: N, P, As and Sb),[7,11] CX_4 (X: F, Cl), and SiY_4 (Y: Cl, Br, and I).[4,8] In the present work, we have extended our calculations to the family of molecules H_2O, H_2S, H_2Se, and H_2Te. We report integral, differential, and momentum transfer elastic cross-sections obtained at the fixed-nuclei static exchange approximation, which agree with available experimental data.

Since all the molecules treated here possess permanent dipole moments, the fixed-nuclei scattering amplitudes diverge in the forward scattering direction ($\theta=0$). Although the SMCPP procedure is useful to overcome this computational limitation, its numerical nature makes it impossible to couple infinite partial waves and, as a result, it will not show the expected divergent behavior in the elastic cross-sections.

This very problem was found in the study of the XH_3 (X=N, P, As, Sb) family, and the following scheme was applied to deal with the long-range dipole moment interaction:[7] the SMCPP method was used to describe the short-range part of the interaction (lower partial waves). Intermediate-range and long-range parts were treated through closure formulas, where the intermediate partial waves were obtained through the first Born full interaction potential. The higher partial waves ($l\rightarrow\infty$) were calculated using the first Born approximation (FBA) of the dipole moment potential. Within the energy range studied ($7.5\,\text{eV}\leqslant E\leqslant 30\,\text{eV}$), it was found that the calculation of such intermediate partial waves is not necessary. The combination of the SMCPP method with the FBA of the dipole moment potential yielded fair results, and, for molecules with small permanent dipole moments (SbH_3, for example), the SMCPP was sufficient, providing faithful cross-sections for $5°\leqslant\theta\leqslant 180°$.

Previous studies on H_2S (Refs. 12–14) reported the existence of a shape resonance at energies around 5 eV at the B_2 symmetry and a broad peak at the A_1 symmetry for energies around 8 eV. In order to seek for these resonances in the integral cross-sections of the heavier molecules, we have also considered energies below 5 eV in our static-exchange calculations.

The theoretical formulation of the method will be given in Sec. II, while Sec. III will deal with computational aspects. The results and discussions will be presented in Sec. IV, and our conclusions will be shown in Sec. V.

II. THEORETICAL FORMULATION

Both SMC[15,16] and SMCPP[3] methods are well discussed in the literature, and only key steps will be given here. The working expression for the scattering amplitude is given by

$$[f_{\vec{k}_i,\vec{k}_f}]=-\frac{1}{2\pi}\sum_{m,n}\langle S_{\vec{k}_f}|V|\chi_m\rangle(A^{(+)-1})_{mn}\langle\chi_n|V|S_{\vec{k}_i}\rangle, \quad (1)$$

where

$$A^{(+)}=\frac{\hat{H}}{N+1}-\frac{(\hat{H}P+P\hat{H})}{2}+\frac{(VP+PV)}{2}-VG_P^{(+)}V. \quad (2)$$

In the above expressions, $S_{\vec{k}_i}$ is the product of a target state and a free wave with momentum $\vec{k}_i$, i.e., a solution of the unperturbed Hamiltonian H_0; V is the interaction potential between the target and the incident electron ($H=H_0+V$); χ_m are $(N+1)$-particle Slater determinants used to expand the trial scattering wave function; $\hat{H}=E-H$ is the total collision energy minus the full Hamiltonian; P is a projection operator onto the open channel space; and $G_P^{(+)}$ is the free-particle Green's function projected onto the P-space. All matrix elements but those of $\langle\chi_m|VG_P^{(+)}V|\chi_n\rangle$, which we call VGV matrix elements, can be calculated analytically. The numerical evaluation of VGV matrix elements[16] is the most time-consuming step of the SMC code, and is drastically reduced with the use of PP.

The Born closure procedure is discussed elsewhere,[17] and we will only give the key steps. The idea is to rotationally resolve the SMCPP elastic scattering amplitudes, and to apply the Born closure procedure for the dipole-allowed $00\rightarrow 10$ rotational excitation. Within the adiabatic nuclei rotation (ANR) approximation, the $J\tau M\rightarrow J'\tau' M'$ rotational excitation scattering amplitude for an asymmetric top will be given by

$$f(J\tau M\rightarrow J'\tau' M';k_{\text{in}},\vec{k}'_{\text{out}})=\langle\Psi^s_{J'\tau' M'}(\Omega)|f^{\text{lab}}(k_{\text{in}},\vec{k}'_{\text{out}},\Omega)|\Psi^s_{J\tau M}(\Omega)\rangle. \quad (3)$$

In the expression above, f^{lab} is the elastic SMCPP scattering amplitude, written in the laboratory-fixed frame (LF); $\Psi^s_{J\tau M}$ is the rotational eigenfunction of an asymmetric top; J is the molecular total angular momentum; M is its projection onto the LF quantization axis; τ is a pseudoquantum number; $\Omega\equiv(\alpha,\beta,\gamma)$ are the Euler angles that define the transformation from the body-fixed frame (BF) to the LF; and $\vec{k}_{\text{in}}$ and $\vec{k}'_{\text{out}}$ are, respectively, incident and outgoing wave vectors, written in the LF.

The FBA rotational scattering amplitude is written as

$$f^{\text{FBA}}(J\tau M\rightarrow J'\tau' M';\vec{k}'_{\text{out}})=\int d\Omega\,\Psi^{s*}_{J'\tau' M'}(\Omega)\,f^{\text{DIP}}_{\text{FBA}}(\beta,\gamma,\vec{k}'_{\text{out}})\Psi^s_{J\tau M}(\Omega), \quad (4)$$

where

$$f^{\text{DIP}}_{\text{FBA}}(\vec{k}_i,\vec{k}_f)=2i\frac{\vec{D}\cdot(\vec{k}_i-\vec{k}'_f)}{|\vec{k}_i-\vec{k}'_f|^2}. \quad (5)$$

It is to be observed that $f^{\text{DIP}}_{\text{FBA}}$ is the dipole moment potential expression for the scattering amplitude in the first Born approximation, and $\vec{D}$, the molecular dipole moment. In order to take long-range effects into account, the Born closure procedure is applied for the dipole-allowed $00\rightarrow 10$ rotational excitation, for which one finds

$$f^{\text{lab}}(J\tau M\rightarrow J'\tau' M';\vec{k}'_{\text{out}})=f^{\text{FBA}}(J\tau M\rightarrow J'\tau' M';\vec{k}'_{\text{out}})+\sum_{l=0}^{l_1}\sum_{\mu}[f^{\text{SMCPP}}_{l\mu}(k_{\text{in}},k_{\text{out}})-f^{\text{FBA}}_{l\mu}(k_{\text{in}},k_{\text{out}})]Y_{l\mu}(\vec{k}'_{\text{out}}), \quad (6)$$

where the coefficients of expansion of Eqs. (3) and (4) are in spherical harmonics (Y_{lm}).

The rotational excitation cross-sections will be given by

$$\frac{d\sigma}{d\Omega}(J\tau\rightarrow J'\tau';\theta'_{\text{out}})=\frac{1}{2\pi}\frac{1}{(2J+1)}\sum_{M=-J}^{J}\sum_{M'=-J'}^{J'}\frac{k_{J'\tau'}}{k_{J\tau}}\times\int_0^{2\pi}d\phi|f_{J\tau M\rightarrow J'\tau' M'}|^2. \quad (7)$$

The elastic cross-section can then be obtained by summing up the rotationally resolved cross-sections. It is a good strategy to use the Born closure in the $00\rightarrow 10$ rotationalexcitation scattering amplitude, instead of in the elastic (unre-

TABLE I. Cartesian Gaussians basis sets.

	H Exponent		O Exponent		S Exponent		Se Exponent		Te Exponent
s	13.236 80	*s*	13.584 83	*s*	7.382 2570	*s*	6.207 805	*s*	4.155 929
s	1.972 460	*s*	6.100 150	*s*	2.063 1670	*s*	1.430 724	*s*	2.903 283
s	0.435 714	*s*	1.149 338	*s*	0.878 0090	*s*	0.648 446	*s*	0.966 967
s	0.109 852	*s*	0.401 369	*s*	0.245 1610	*s*	0.267 016	*s*	0.657 771
		s	0.137 458	*s*	0.061 6300	*s*	0.087 372	*s*	0.199 320
				s	0.015 5600	*s*	0.042 807	*s*	0.059 653
p	0.341 264	*p*	10.336 98	*p*	6.757 3730	*p*	5.451 587	*p*	3.841 243
p	0.080 694	*p*	2.918 040	*p*	2.086 9100	*p*	1.715 577	*p*	1.075 123
p	0.026 822	*p*	0.938 357	*p*	0.692 7260	*p*	0.421 179	*p*	0.578 687
		p	0.316 141	*p*	0.268 6020	*p*	0.127 967	*p*	0.275 698
		p	0.109 323	*p*	0.095 9360	*p*	0.029 344	*p*	0.138 669
				p	0.021 4860	*p*	0.013 107	*p*	0.083 686
		d	1.698 204	*d*	1.689 0350	*d*	0.522 708	*d*	1.831 258
		d	0.455 259	*d*	0.476 3170	*d*	0.200 190	*d*	0.248 219
		d	0.146 894	*d*	0.151 5580	*d*	0.079 288	*d*	0.090 505

solved) scattering amplitude, because it is possible to take advantage of the rotational energy transfer to make $|\vec{k}_{\text{in}}| \neq |\vec{k}'_{\text{out}}|$ in Eq. (5), therefore avoiding divergence in the differential cross-sections at $\theta = 0$.

III. COMPUTATIONAL PROCEDURES

In our calculations, the valence part of the target state was described by a single configuration wave-function, obtained at the Hartree–Fock approximation, in which no correlation effects are included. However, by construction, the PP includes core–core and core–valence correlation.[9] The Cartesian Gaussian basis sets employed in the description of the target and in the representation of the scattering orbitals are shown in Table I. For the water molecule, extra scattering basis functions were added: one *p* (exponent 0.027 331) function on the O atom; one *s* function (exponent 0.045 819) on the mid-point of the line joining the H atoms; and one *s* function (exponent 0.045 819) centered on the point obtained by reflection of the coordinates of the last extra *s* function on the O*xy* plane. As a result, we have used a 68 function basis set to describe the $e^- - H_2O$ scattering process. For all atoms, the basis sets were generated by a variational method,[18] where linear combinations of Gaussian functions are fitted to the radial atomic pseudowavefunctions. For the heavier molecules, scattering orbitals are distributed by symmetry as follows: 29 for A_1, 18 for B_2, 11 for B_1, and 6 for A_2. For water, one finds: 31 for A_1, 19 for B_2, 12 for B_1, and 6 for A_2. All calculations were performed at the experimental geometries, given in Table II. Calculated and experimental dipole moments are shown in Table III.

IV. RESULTS AND DISCUSSION

The water molecule has been widely studied both theoretically[19–25] and experimentally.[26–29] We will therefore briefly present our new calculations only for completeness.

In Figs. 1 and 2, we show elastic (rotationally summed) differential cross-sections (DCS) for H_2O at 2, 4, 6, 8, 10, 15, 20, and 30 eV. Although obtained at the static-exchange (SE) level of approximation, we believe that these results are reliable even at the lower energies. Previous work[20–22] has shown that polarization effects are not important for this molecule. Our results were calculated in two ways: (a) SMCPP only (rotationally unresolved); and (b) SMCPP with Born closure (rotationally summed). As expected, the long-range interactions are very important for this molecule. Even at 30 eV, there are significant discrepancies between results with and without Born closure at $0 < \theta \leqslant 30°$. We also compare our results with other SE (Ref. 21) and SE plus polarization (Ref. 22) calculations. Experimental data of Refs. 26–29 are also shown. There is a reasonable agreement among theoretical results. That can be understood as another indication of the irrelevance of polarization effects. At lower energies ($E \leqslant 8$ eV), our results are larger than those of Machado *et al.*[21] and those of Rescigno and Lengsfield.[22] In general, one finds good agreement between calculated and experimental results.

TABLE II. Molecular geometries.[a]

System	H–X–H angle (deg)	X–H bond length (Å)
H_2O	104.5	0.958
H_2S	92.2	1.336
H_2Se	90.6	1.460
H_2Te	90.3	1.658

[a]Reference 38.

TABLE III. Experimental and calculated dipole moments (Debye).

System	Experimental	Calculated
H_2O	1.84	1.990
H_2S	0.97	1.129
H_2Se	0.24	0.755
H_2Te	<0.2	0.243

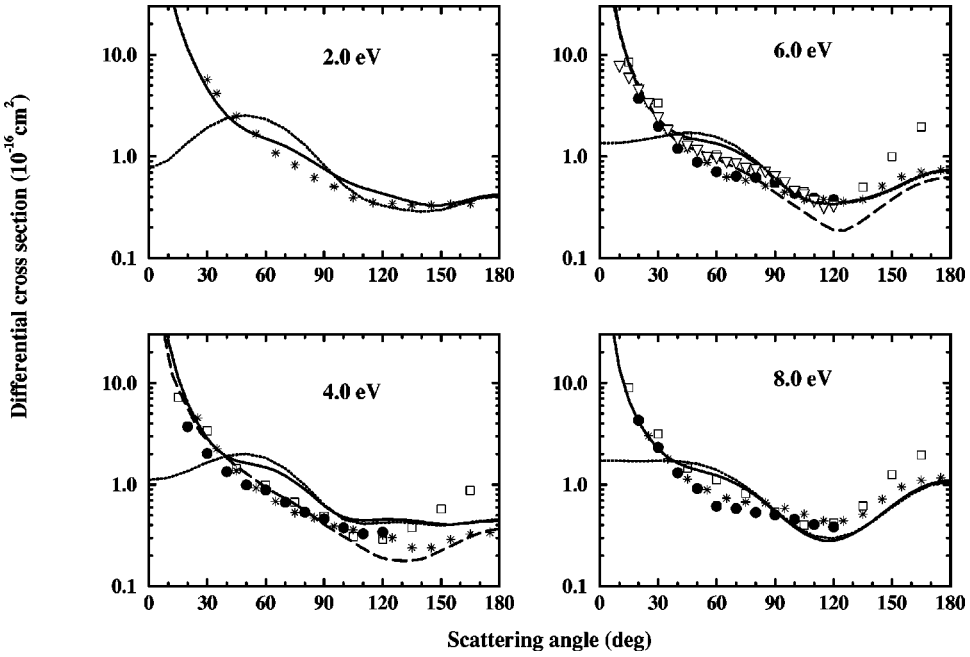

FIG. 1. Elastic differential cross-section for H_2O at 2, 4, 6, and 8 eV. Full line: present results (SMCPP with Born closure); dotted line: present results (SMCPP only); stars: SEP results of Ref. 22; dashed line: SE results of Ref. 21; bullets: experimental data of Ref. 26; open squares: experimental data of Ref. 27; open triangles: experimental data of Ref. 29.

In Fig. 3, and also in Tables IV and V, we show integral and momentum transfer cross-sections (ICS and MTCS) for water with and without Born closure, along with experimental data of Refs. 26–29. Once again, SMCPP results are rotationally unresolved, while SMCPP+FBA results are rotationally summed. Rotationally summed ICS with Born closure of Gianturco *et al.*[25] is also shown. One can notice some disagreement among experimental results. Our results, however, generally lie within error bars of Ref. 29. The ICS of Gianturco *et al.* is overestimated. Comparison between ICS with and without Born closure confirms that long-range effects play an important role in electron collisions against H_2O.

In Fig. 4 we show ICS and MTCS for H_2S. The results are also presented in Tables IV and V, respectively. Our cross-sections were again calculated with (rotationally summed) and without (rotationally unresolved) Born closure. For comparison purposes, we also show other theoretical results[13,14,30] and experimental data.[31] Although our ICS is a little higher than the experiment, it often lies within the error bars. There is also good agreement among theoretical ICS, but results of Machado *et al.*[14] presents a structure around 8 eV that is not noticed in the other calculations. One also finds very good agreement among theoretical MTCS, but, in general, the calculated cross-sections are higher than the experimental result. It is interesting to observe that long-range effects are much more modest for $e^- - H_2S$ scattering than for the water molecule.

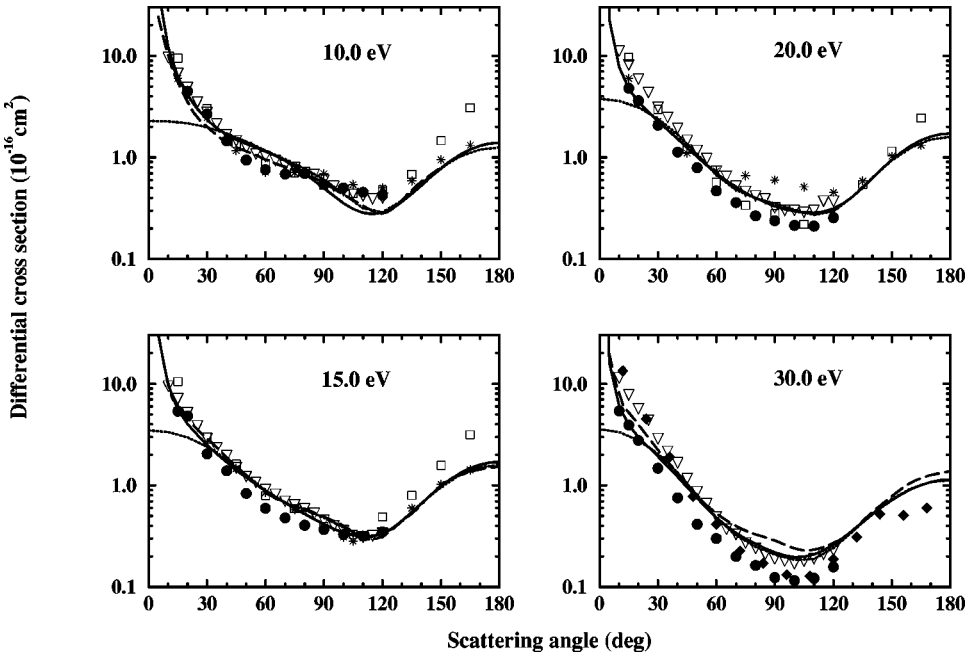

FIG. 2. Elastic differential cross-section for H_2O at 10, 15, 20, and 30 eV. Same legends as Fig. 1. Diamonds (30 eV) are experimental data of Ref. 28.

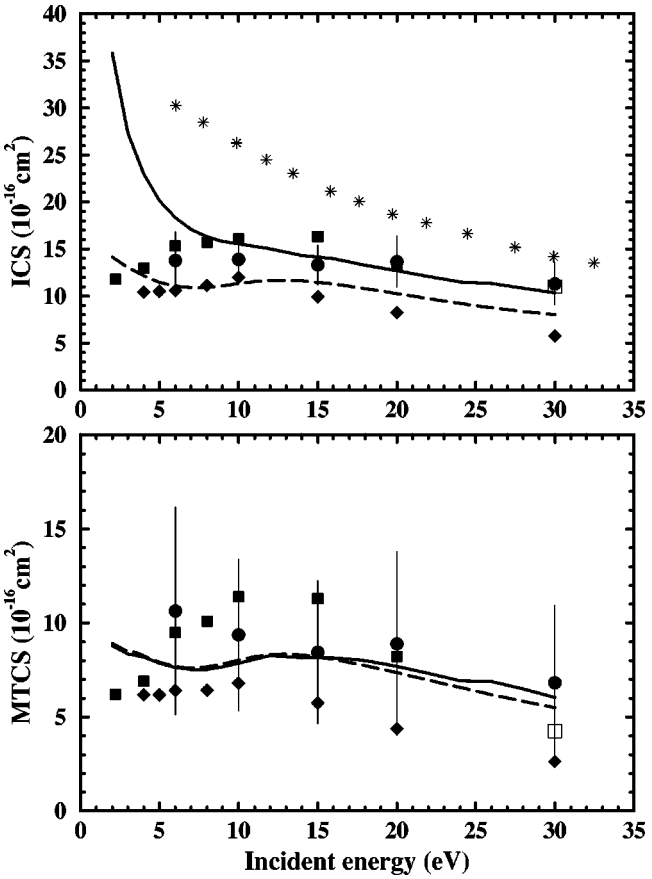

FIG. 3. Elastic integral and momentum transfer cross-section for H_2O. Full line: present results (SMCPP with Born closure); long-dashed line: present results (SMCPP only); stars: SEP results of Ref. 25; filled diamonds: experimental data of Ref. 26; filled squares: experimental data of Ref. 27; circles with error bars: experimental data of Ref. 29; open square: experimental data of Ref. 28.

TABLE IV. Elastic integral cross-sections (10^{-16} cm^2) for H_2X.

Energy (eV)	H_2O[a]	H_2S[a]	H_2Se[b]	H_2Te[b]
2.0	35.85			
3.0	27.33			
4.0	22.96			
5.0	20.15	32.92	37.58	48.34
6.0	18.33	32.38	38.49	47.20
7.0	17.10	32.53	38.64	44.99
8.0	16.30	32.55	37.99	42.36
9.0	15.82	32.26	36.86	39.70
10.0	15.54	31.68	35.52	37.18
12.0	15.00	29.98	32.68	32.71
14.0	14.29	27.92	29.94	28.89
16.0	13.97	25.86	27.39	25.61
18.0	13.27	23.97	25.05	22.77
20.0	12.69	22.31	22.95	20.32
22.0	12.08	20.93	21.07	18.20
24.0	11.49	19.68	19.37	16.38
26.0	11.34	18.55	17.84	14.80
28.0	10.82	17.52	16.45	13.44
30.0	10.35	16.56	15.17	12.26

[a]With Born closure.
[b]Without Born closure.

TABLE V. Elastic momentum transfer cross-sections (10^{-16} cm^2) for H_2X.

Energy (eV)	H_2O[a]	H_2S[a]	H_2Se[b]	H_2Te[b]
2.0	8.782			
3.0	8.351			
4.0	8.190			
5.0	7.858	22.23	27.77	32.45
6.0	7.630	21.30	27.41	28.52
7.0	7.518	20.58	26.02	24.59
8.0	7.533	19.55	24.06	21.19
9.0	7.664	18.30	22.01	18.44
10.0	7.855	16.97	20.10	16.24
12.0	8.267	14.43	16.87	13.03
14.0	8.156	12.32	14.30	10.79
16.0	8.151	10.68	12.26	9.121
18.0	7.996	9.418	10.64	7.827
20.0	7.684	8.435	9.362	6.802
22.0	7.319	7.849	8.360	5.979
24.0	6.930	7.248	7.564	5.310
26.0	6.883	6.762	6.917	4.763
28.0	6.497	6.367	6.359	4.315
30.0	6.031	6.041	5.833	3.946

[a]With Born closure.
[b]Without Born closure.

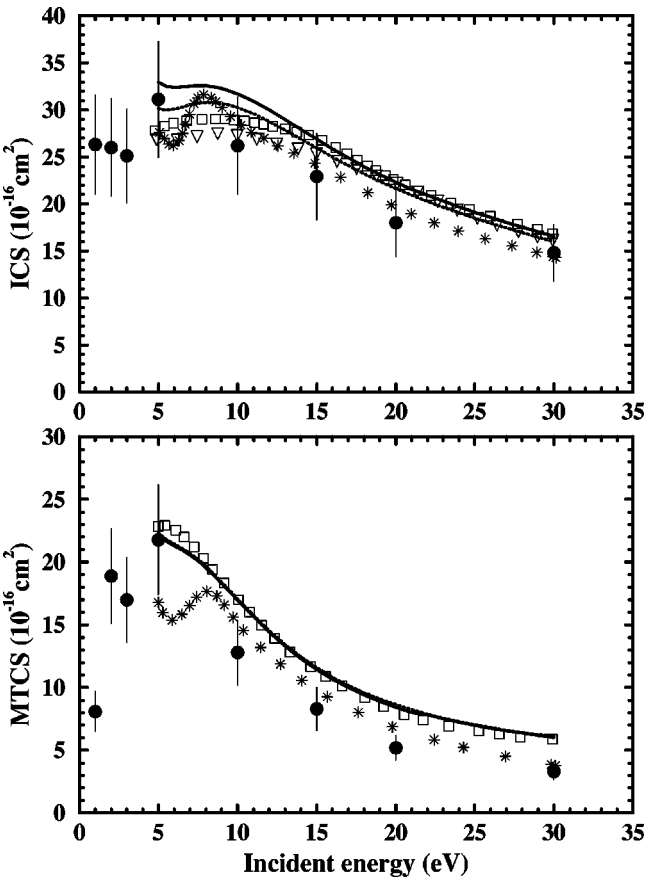

FIG. 4. Elastic integral and momentum transfer cross-sections for H_2S. Full line: present results (SMCPP with Born closure); dotted line: present results (SMCPP only); stars: SE results of Ref. 14; open squares: SEP results of Ref. 30; open triangles: SEP results of Ref. 13; bullets: experimental data of Ref. 31.

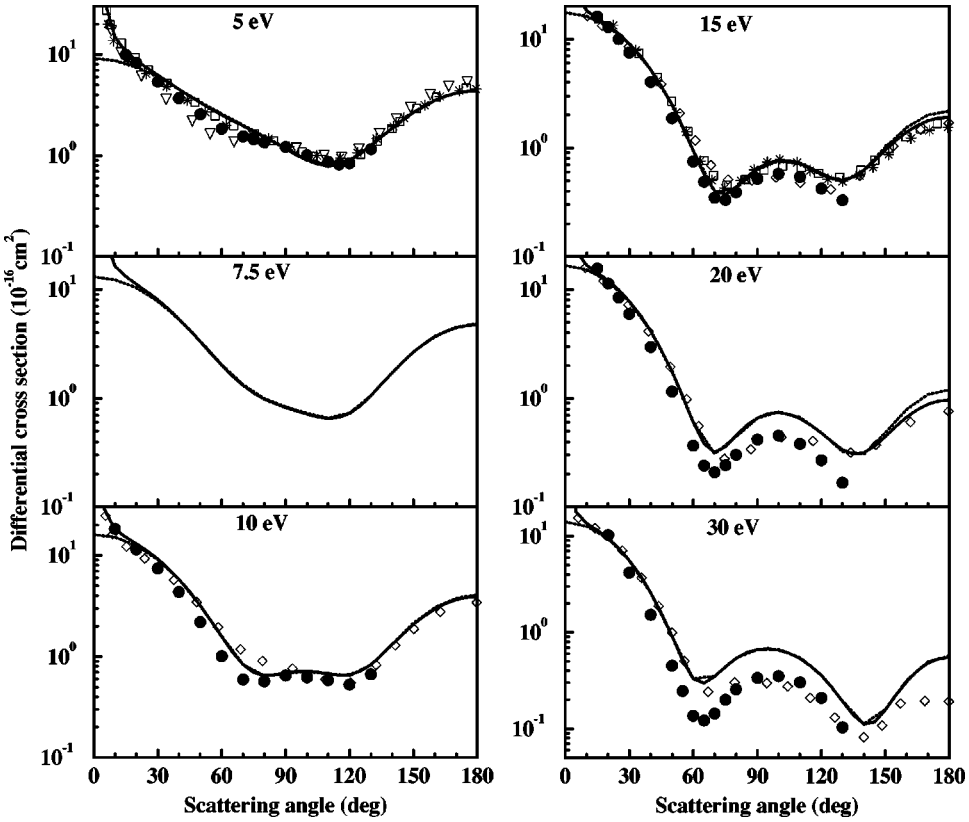

FIG. 5. Elastic differential cross-sections for H_2S at 5, 7.5, 10, 15, 20, and 30 eV. Full line: present results (SMCPP with Born closure); dotted line: present results (SMCPP only); open squares: SE results of Ref. 30; open triangles: SEP results of Ref. 30; open diamonds: SE results of Ref. 14; stars: SEP results of Ref. 32; bullets: experimental data of Ref. 31.

DCS for H_2S is presented in Fig. 5, along with experimental data of Gulley *et al.*[31] and calculations of Refs. 14, 30, 32. Our results are again presented in two ways: rotationally summed DCS with Born closure, and rotationally unresolved DCS without FBA. There is a very good agreement among theoretical results. Agreement with experimental data is always found in shape, but there are some discrepancies in magnitude at 20 and 30 eV. It is also interesting to note that

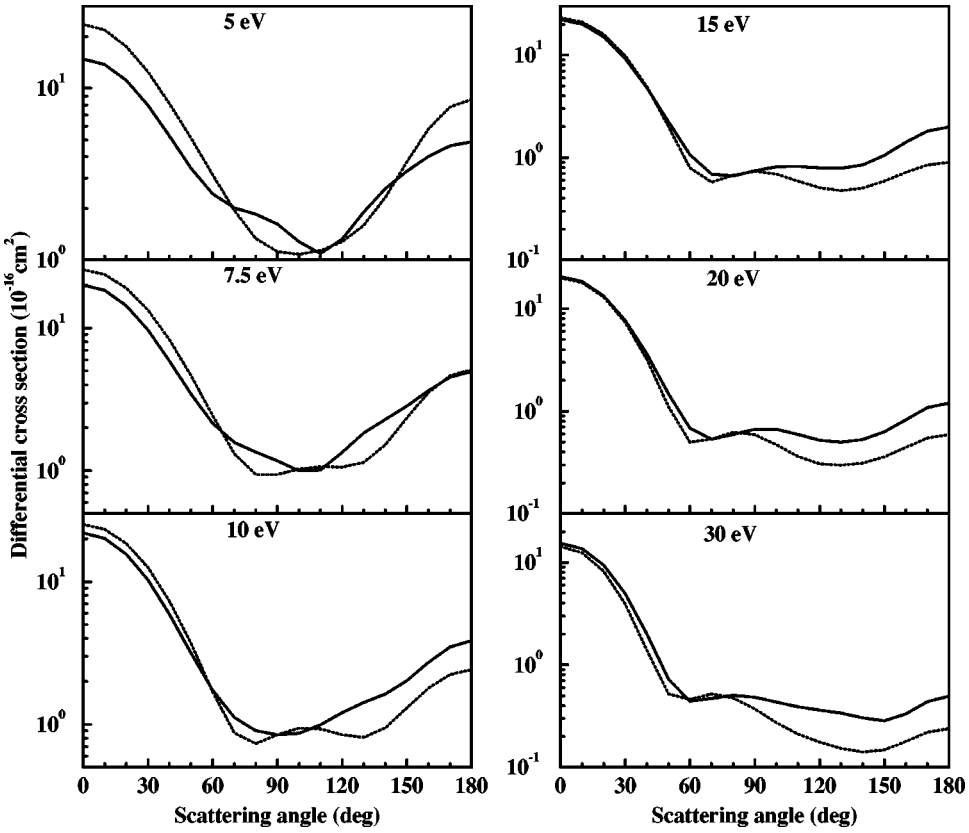

FIG. 6. Elastic differential cross-sections for H_2Se and H_2Te at 5, 7.5, 10, 15, 20, and 30 eV. Full line: H_2Se (SMCPP only); long dashed line: H_2Te (SMCPP only).

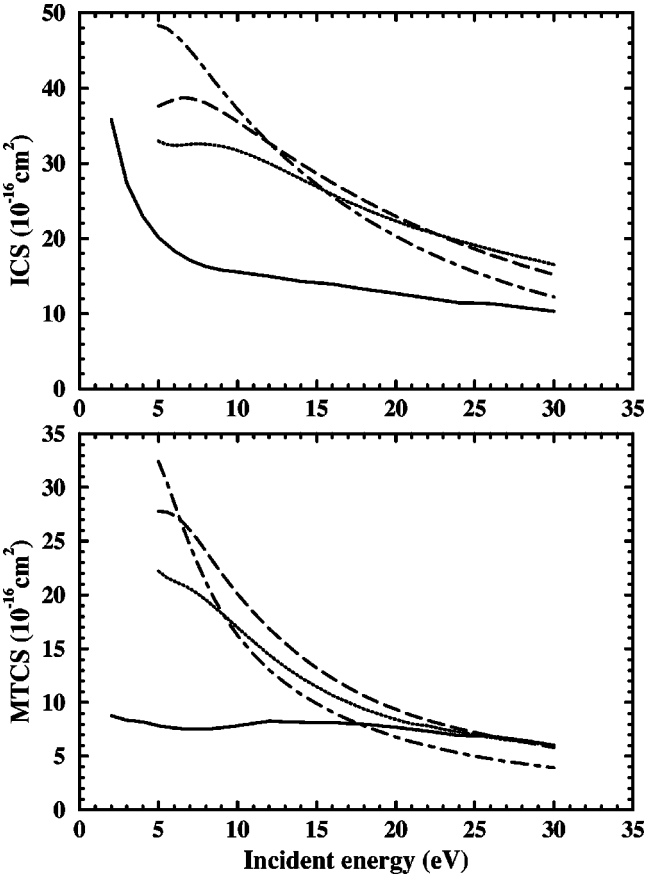

FIG. 7. Elastic integral and momentum transfer cross-sections for H_2X. Full line: H_2O (SMCPP with Born closure); dotted line: H_2S (SMCPP with Born closure); long-dashed line: H_2Se (SMCPP only); dot-dashed line: H_2Te (SMCPP only).

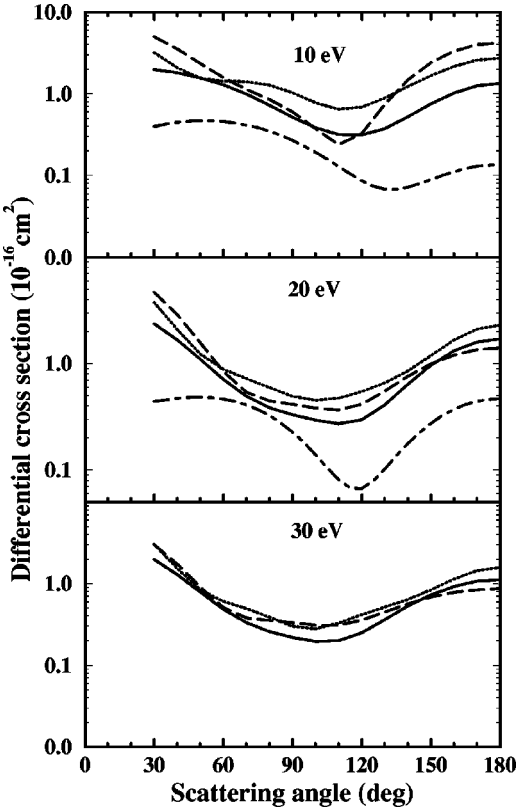

FIG. 8. Elastic differential cross-sections for isoelectronic systems at 10, 20, and 30 eV. Solid line: H_2O; dotted line: NH_3; long-dashed line: CH_4; dot-dashed line: Ne atom (Ref. 33).

our calculations with Born closure (5 and 10 eV) are closer to the experimental points near the forward scattering direction. There is no difference between the results with and without Born closure for $\theta > 20°$. For energies above 10 eV, we find two minima in the DCS, meaning that the central atom is heavy enough to cause d-wave scattering.

Figure 6 shows the DCS for H_2Se and H_2Te. Due to the modest dipole moments, the FBA did not provide significant contributions, and we show SMCPP calculations for both systems. We also find d-wave behavior in the DCS for $E \geqslant 7.5$ eV, for H_2Te, and for $E \geqslant 15$ eV for H_2Se. This behavior was also found for AsH_3 and SbH_3,[11] which are isoelectronic to H_2Se and H_2Te, respectively. SnH_4, which is isoelectronic to SbH_3 and H_2Te, was found to cause partial f-wave scattering ($E \geqslant 20$ eV).[10]

ICS and MTCS (SMCPP only) for H_2Se and H_2Te are shown in Fig. 7 and also in Tables IV and V. Results of H_2O and H_2S (both with FBA) are also included for comparison purposes. For $5 \leqslant E \leqslant 10$ eV, one finds that less polar molecules (H_2Se and H_2Te) have larger ICS than H_2S and H_2O. In the H_2X family, the dipole moment magnitude decreases as the central atom size increases. As a result, one finds two counterbalancing aspects determining the ICS magnitude: molecular dipole moment and molecular size. Although H_2S and H_2O present, respectively, intermediate and large dipole

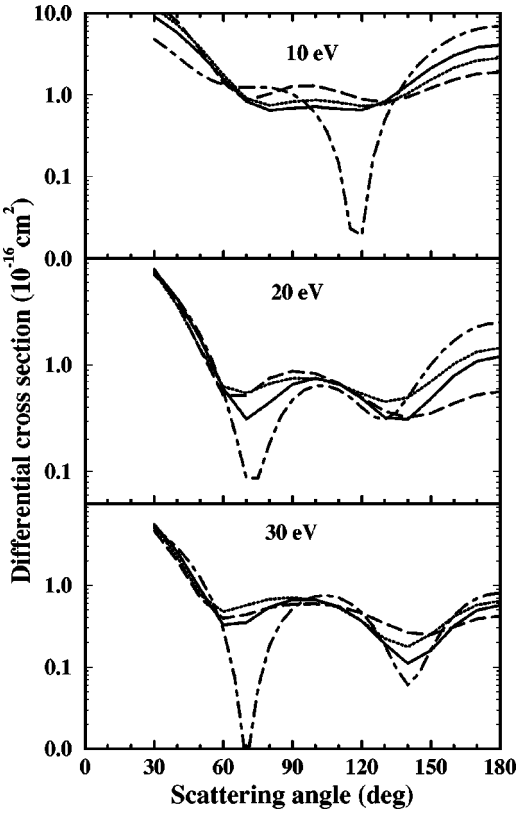

FIG. 9. Elastic differential cross-sections for isoelectronic systems at 10, 20, and 30 eV. Solid line: H_2S; dotted line: PH_3; long-dashed line: SiH_4; dot-dashed line: Ar atom (Ref. 34).

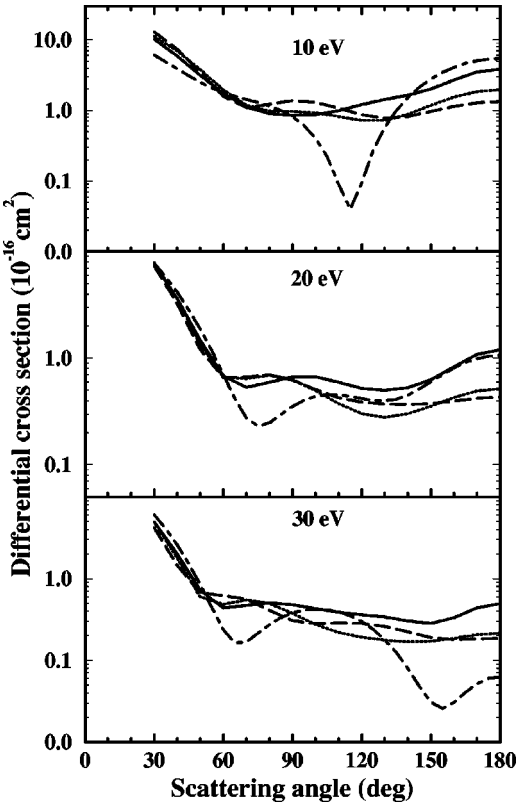

FIG. 10. Elastic differential cross-sections for isoelectronic systems at 10, 20, and 30 eV. Solid line: H_2Se; dotted line: AsH_3; long-dashed line: GeH_4; dot-dashed line: Kr atom (Ref. 35).

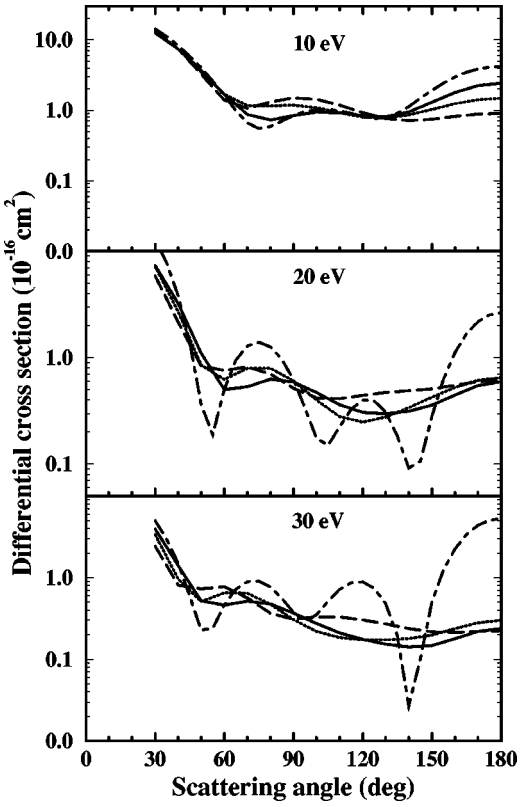

FIG. 11. Elastic differential cross-sections for isoelectronic systems at 10, 20, and 30 eV. Solid line: H_2Te; dotted line: SbH_3; long-dashed line: SnH_4; dot-dashed line: Xe atom (Ref. 36).

moments, our calculations show that ICS are dominated by molecular size. In other words, one could say that, at lower energies ($5\,\text{eV} < E < 10\,\text{eV}$), where long-range effects are known to be relevant, the size of the molecule leads to a more effective interaction than the dipole moment potential does. For the higher energies, the cross-sections do not follow a clear hierarchy of molecular sizes.

In previous papers concerning XH_3 (X: N, P, As, Sb) and XH_4 (X: C, Si, Ge, Sn, Pb) families,[11,10] it was observed that hydrogen atoms did not significantly act as scattering centers, and that cross-sections were strongly affected by central atom sizes. This seems to hold for H_2X molecules, as discussed above. In order to illustrate the role of central atom size and of H atoms in the scattering process, we show, in Figs. 8–11, DCS for isoelectronic systems at 10, 20, and 30 eV. The systems are Ne atom (Ref. 33 result), H_2O, NH_3, CH_4 (Fig. 8); Ar atom (Ref. 34 result), H_2S, PH_3, SiH_4 (Fig. 9); Kr atom (Ref. 35 result), H_2Se, AsH_3, GeH_4 (Fig. 10); Xe atom (Ref. 36 result), H_2Te, SbH_3, SnH_4 (Fig. 11). For all systems, we show SMCPP calculations (without FBA) for $\theta \geqslant 30°$, in order to minimize the influence of molecular dipole moments in the DCS. There are two striking features: (i) at a given energy, molecular DCS (of H_2X, XH_3, and XH_4 molecules) are very similar within each group of isoelectronic systems; (ii) the atomic DCS (of the rare gas elements isoelectronic with the molecules) are always dissimilar, presenting, in general, more structures (oscillation and minima). With these two facts in mind, one should assert that, as long as electron–molecule scattering is concerned, H atoms do not play relevant roles in the collision process. Instead of that, these atoms seem to mainly act as electron donors to the central atoms, which determine the most relevant features of the cross-sections. When atomic and molecular DCS are compared within an isoelectronic group, however, one finds an interesting contribution of H atoms. In e^--atom scattering, the interaction potential is spherically symmetric. As a result, the incident direction is irrelevant. In e^--molecule collisions, however, this is no longer true, and one has to average over all possible incident directions, to take into account the random molecular orientation found in a discharge environment. For a given incident direction, there will be some structures in the DCS. For a slightly different incident direction, the structures will change a little bit. As a consequence, when one averages over all possible orientations, the interference of all structures will lead to smoother cross-sections, as observed in Figs. 8–11. A similar discussion has been carried out in a previous work on e^--O_2 scattering,[37] where a comparison between angularly averaged and unaveraged cross-sections is found. Hence, even though H atoms do not strongly act as scattering centers, they make e^--molecules collisions anisotropic, leading to smoother DCS. It is to be emphasized that such smoothing effect is not only a theoretical mean result. In real gases, the molecular orientation is aleatory, and experimental cross-sections will be inherently averaged.

We have investigated the integral cross-sections for en-

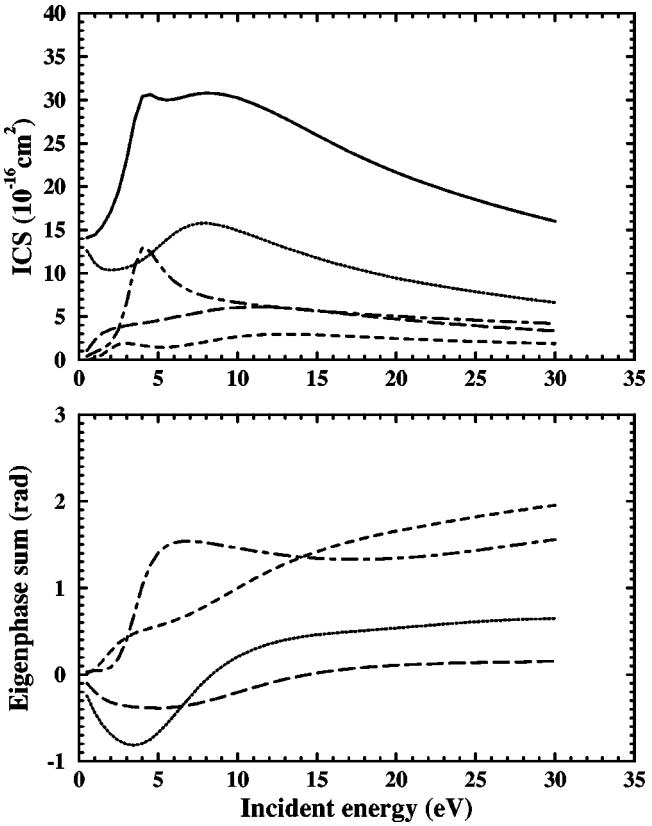

FIG. 12. Integral cross-section and its symmetry decomposition for H_2S (upper plot) and eigenphase sum (lower plot). Full line: elastic ICS; dotted line: A_1 symmetry; short-dashed line: A_2 symmetry; long-dashed line: B_1 symmetry; dot-dashed line: B_2 symmetry.

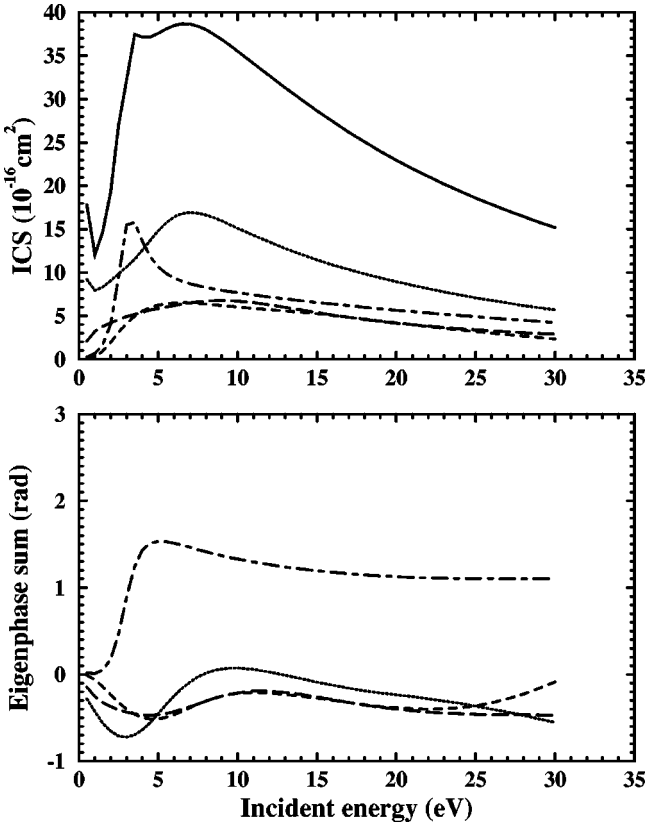

FIG. 13. Integral cross-section and its symmetry decomposition for H_2Se (upper plot) and eigenphase sum (lower plot). Same captions as Fig. 12.

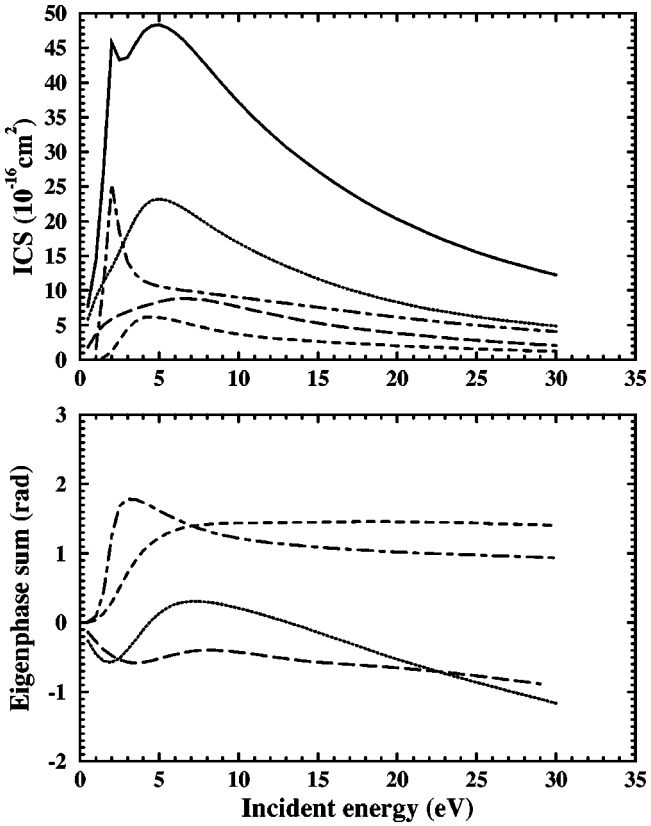

FIG. 14. Integral cross-section and its symmetry decomposition for H_2Te (upper plot) and eigenphase sum (lower plot). Same captions as Fig. 12.

ergies below 5 eV looking for possible shape resonances for H_2S, H_2Se, and H_2Te. Through the symmetry decomposition of the cross-sections and eigenphase sum analysis we found shape resonances for all molecules at the B_2 symmetry. For H_2Te we also found a shape resonance at the A_2 symmetry. A very broad feature was also seen at the A_1 symmetry for all molecules. These results are shown in Figs. 12, 13, and 14 for H_2S, H_2Se, and H_2Te, respectively. In Table VI we show the position of the structures for these molecules. In each symmetry the peaks move down in energy, accordingly the size of the X atom grows up.

The results for H_2Te presented in this work differ substantially from the results of previous calculations,[11] for energies lower than 10 eV. We attribute these differences to linear dependency in the basis set used in those calculations. In fact we have repeated those calculations without including the $(x^2+y^2+z^2)\exp(-\alpha r^2)$ components of the basis set as scattering orbitals, and the results become identical to those shown here. The results of this procedure are shown in Fig. 15, for the integral cross-section, and in Fig. 16 for the DCS. Though not shown here, similar observations hold for H_2O.

TABLE VI. Approximate position of the structures (eV).

System	A_1	B_2	A_2
H_2S	8.0	4.0	···
H_2Se	7.0	3.5	···
H_2Te	5.0	2.0	4.5

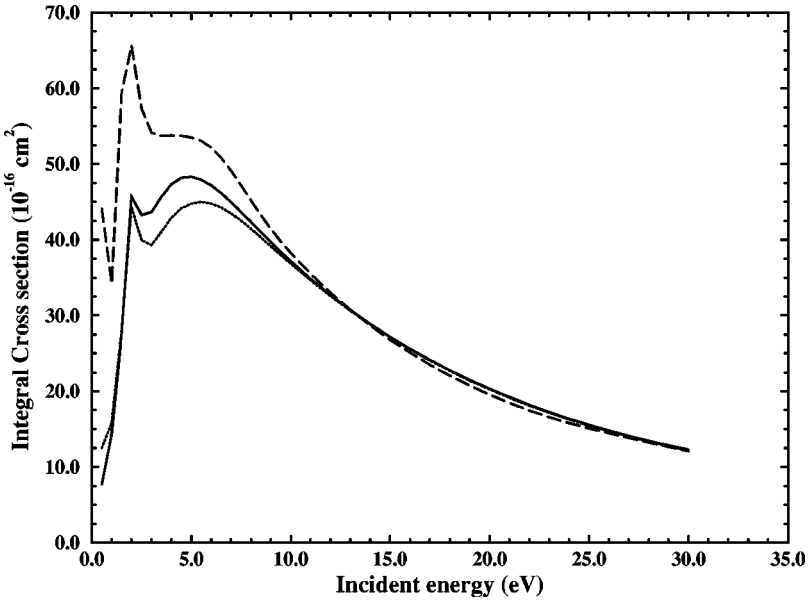

FIG. 15. Integral cross-section for H_2Te obtained with different basis sets. Full line: present results; dashed line: SMCPP calculation of Ref. 11; dotted line: SMCPP calculation of Ref. 11 without the symmetric *d*-function linear combination (see text for explanation).

We have repeated this procedure for H_2S and H_2Se, and found that the results were not affected. A detailed discussion about linear dependency in scattering calculations caused by the $(x^2+y^2+z^2)\exp(-\alpha r^2)$ components of the basis set has been carried out elsewhere.[8]

V. CONCLUSIONS

We have reported elastic differential, integral, and momentum transfer cross-sections for electrons scattering by H_2X (X: O, S, Se, and Te) at the static exchange level of approximation, with the incident energy ranging from 5 up to 30 eV. Since polarization effects are not important for H_2O (the highly polar molecule of the family), we also reported cross-sections from 2 to 5 eV for this molecule. Since the systems present permanent dipole moments, we have combined SMCPP method with a Born closure procedure.

Our calculated cross-sections for H_2O and H_2S are in good agreement with other theoretical results. Agreement with available experimental data is also encouraging.

It was found that molecular size is a more relevant feature than dipole moments in determining the magnitude of integral cross-sections at low energies ($5\ \text{eV} \leqslant E \leqslant 10\ \text{eV}$). Comparison among isoelectronic systems showed that the central atoms are the effective scattering centers in electron collisions against H_2X (X: O, S, Se, Te), XH_3 (X: N, P, As, Sb), and XH_4 (X: C, Si, Ge, Sn). Although H atoms are not strong scatterers, they make e^--molecule scattering anisotropic. As a result, the structures found in the differential cross-sections for each incident direction, cancel out when the random target orientation is taken into account, leading to smoother cross-sections.

Shape resonances were found at the B_2 symmetry for

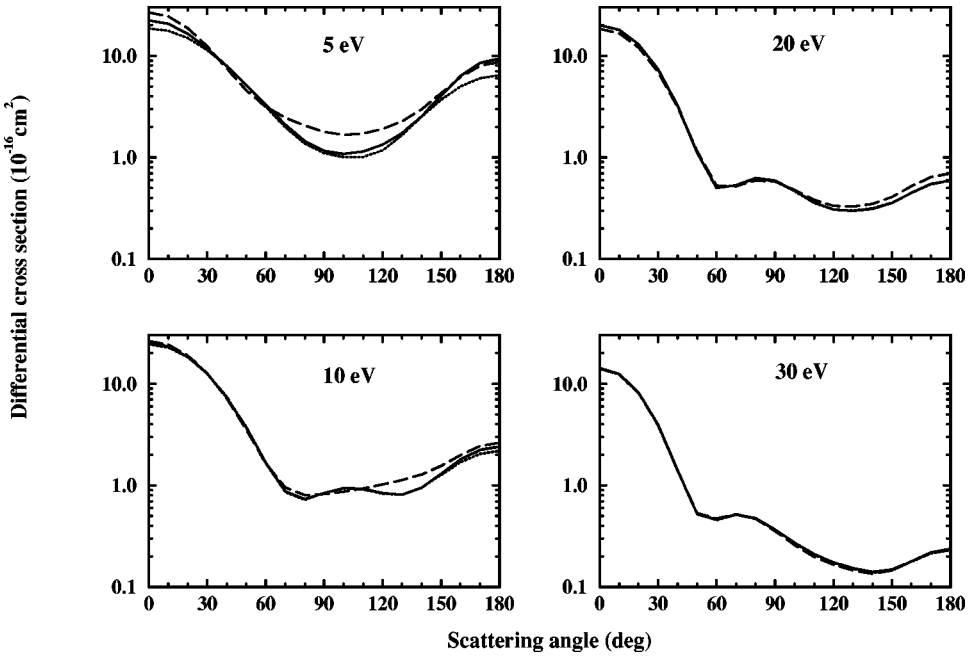

FIG. 16. Differential cross-section for H_2Te obtained with different basis sets. Full line: present results; dashed line: SMCPP calculation of Ref. 11; dotted line: SMCPP calculation of Ref. 11 without the symmetric *d*-function linear combination (see text for explanation).

H_2S, H_2Se, and H_2Te. For H_2Te, a shape resonance at the A_2 symmetry was also found. All molecules presented a very broad structure at the A_1 symmetry.

ACKNOWLEDGMENTS

M.H.F.B, M.A.P.L., and L.G.F. acknowledge support from Brazilian agency CNPq. M.T. do N.V. acknowledges support from Brazilian agency FAPESP. M.H.F.B. also acknowledges partial support from FUNPAR. Our calculations were performed at CCE-UFPR and CENAPAD-SP.

[1] K. Takayanagi and K. Itikawa, Adv. At. Mol. Phys. **VI**, 105 (1970).
[2] A. Garscadden, Z. Phys. D **24**, 97 (1992). (All articles in this issue are devoted to relevant phenomena that take place in cold plasma.)
[3] M. H. F. Bettega, L. G. Ferreira, and M. A. P. Lima, Phys. Rev. A **47**, 1111 (1993).
[4] A. P. P. Natalense, M. H. F. Bettega, L. G. Ferreira, and M. A. P. Lima, Phys. Rev. A **52**, R1 (1995).
[5] A. P. P. Natalense, M. H. F. Bettega, L. G. Ferreira, and M. A. P. Lima, Phys. Rev. A **59**, 879 (1999); M. H. F. Bettega, M. T. do N. Varella, L. G. Ferreira, and M. A. P. Lima, J. Phys. B **31**, 4419 (1998); M. H. F. Bettega, M. A. P. Lima, and L. G. Ferreira, *ibid.* **31**, 2091 (1998); M. H. F. Bettega, A. J. S. Oliveira, A. P. P. Natalense, M. A. P. Lima, and L. G. Ferreira, Eur. Phys. J. D **1**, 291 (1998); M. T. do N. Varella, L. G. Ferreira, and M. A. P. Lima, J. Phys. B **32**, 2031 (1999).
[6] M. T. do N. Varella, M. H. F. Bettega, and M. A. P. Lima, Z. Phys. D **39**, 59 (1997).
[7] M. T. do N. Varella, M. H. F. Bettega, A. J. R. da Silva, and M. A. P. Lima, J. Chem. Phys. **110**, 2452 (1999).
[8] M. T. do N. Varella, A. P. P. Natalense, M. H. F. Bettega, and M. A. P. Lima, Phys. Rev. A (accepted).
[9] G. B. Bachelet, D. R. Hamann, and M. Schlüter, Phys. Rev. B **26**, 4199 (1982).
[10] M. H. F. Bettega, A. P. P. Natalense, M. A. P. Lima, and L. G. Ferreira, J. Chem. Phys. **103**, 10566 (1995).
[11] M. H. F. Bettega, M. A. P. Lima, and L. G. Ferreira J. Chem. Phys. **105**, 1029 (1996).
[12] A. Jain and D. G. Thompson, J. Phys. B **17**, 443 (1983).
[13] F. A. Gianturco, J. Phys. B **24**, 4627 (1991).
[14] L. E. Machado, E. P. Leal, L. Mu-Tao, and L. M. Brescansin, J. Mol. Struct.: THEOCHEM **335**, 37 (1995).
[15] K. Takatsuka and V. McKoy, Phys. Rev. A **24**, 2473 (1981); *ibid.* **30**, 1734 (1984).
[16] M. A. P. Lima and V. McKoy, Phys. Rev. A **38**, 501 (1988); M. A. P. Lima, L. M. Brescansin, A. J. R. da Silva, K. Winstead, and V. McKoy, *ibid.* **41**, 327 (1990).
[17] A. P. P. Natalense, M. T. do N. Varella, M. H. F. Bettega, L. G. Ferreira, and M. A. P. Lima, J. Phys. B (submitted).
[18] M. H. F. Bettega, A. P. P. Natalense, M. A. P. Lima, and L. G. Ferreira, Int. J. Quantum Chem. **60**, 821 (1996).
[19] L. M. Brescansin, M. A. P. Lima, T. L. Gibson, V. McKoy, and W. M. Huo, J. Chem. Phys. **85**, 1854 (1986).
[20] R. Greer and D. Thompson, J. Phys. B **27**, 3533 (1994).
[21] L. E. Machado, L. Mu-Tao, L. M. Brescansin, M. A. P. Lima, and V. McKoy, J. Phys. B **28**, 467 (1995).
[22] T. N. Rescigno and B. H. Lengsfield, Z. Phys. D **24**, 117 (1992).
[23] F. A. Gianturco, J. Phys. B **24**, 3837 (1991).
[24] J. Yuan and Z. Zhang, Phys. Rev. A **45**, 4565 (1992).
[25] F. A. Gianturco, S. Meloni, P. Paioletti, R. R. Lucchese, and N. Sanna, J. Chem. Phys. **108**, 4002 (1998).
[26] A. Danjo and H. Nishimura, J. Phys. Soc. Jpn. **54**, 1224 (1985).
[27] T. W. Shyn and S. Y. Cho, Phys. Rev. A **36**, 5138 (1987).
[28] T. W. Shyn and A. Grafe, Phys. Rev. A **46**, 4406 (1992).
[29] W. M. Johnstone and W. R. Newell, J. Phys. B **24**, 3633 (1991).
[30] B. H. Lengsfield, T. N. Rescigno, C. W. McCurdy, and S. Parker (1992), as quoted in Ref. 31.
[31] R. J. Gulley, M. J. Brunger, and S. J. Buckman, J. Phys. B **26**, 2913 (1992).
[32] T. Nishimura and Y. Itikawa, J. Phys. B **29**, 4213 (1996).
[33] H. P. Saha, Phys. Rev. A **39**, 5048 (1989).
[34] J. E. Sienkiewicz and W. E. Baylis, J. Phys. B **20**, 5145 (1987).
[35] J. E. Sienkiewicz and W. E. Baylis, J. Phys. B **25**, 2081 (1992).
[36] R. P. McEachran and A. D. Stauffer, J. Phys. B **17**, 2507 (1984).
[37] F. J. da Paixão Filho, M. A. P. Lima, and V. McKoy, Phys. Rev. Lett. **68**, 1698 (1992).
[38] W. J. Hehre, L. Radom, P. v. R. Schleyer, and J. A. Pople, *Ab Initio Molecular Orbital Theory* (John Wiley & Sons, New York, 1986).